Inorganic Chemistry

Article

pubs.acs.org/IC

A Novel Efficient Mn^{4+} Activated $Ca_{14}Al_{10}Zn_6O_{35}$ Phosphor: Application in Red-Emitting and White LEDs

Wei Lü,*[,†] Wenzhen Lv,[†,‡] Qi Zhao,[†,‡] Mengmeng Jiao,[†,‡] Baiqi Shao,[†,‡] and Hongpeng You*[,†]

[†]State Key Laboratory of Rare Earth Resource Utilization, Changchun Institute of Applied Chemistry, Chinese Academy of Sciences, Changchun 130022, P. R. China

[‡]University of the Chinese Academy of Sciences, Beijing 100049, P. R. China

ABSTRACT: A new, highly efficient deep red-emitting phosphor $Ca_{14}Al_{10}Zn_6O_{35}:Mn^{4+}$ was developed as a component of solid-state white light-emitting diodes (LEDs). The structural and optical characterization of the phosphor is described. The phosphor exhibits strong emission in the range of 650−700 nm when excited by 460 nm excitation, with a quantum efficiency approaching 50%. Concentration dependence of Mn^{4+} luminescence in $Ca_{14}Al_{10}Zn_6O_{35}:Mn^{4+}$ is investigated. Attempts to understand the thermal stability on the basis of the thermal quenching characteristics of $Ca_{14}Al_{10}Zn_6O_{35}:Mn^{4+}$ is presented. The results suggest that phosphors deriving from $Ca_{14}Al_{10}Zn_6O_{35}:Mn^{4+}$ have potential application for white LEDs. In addition, influence of cation substitution on the luminescence intensity of these phosphors is elucidated.

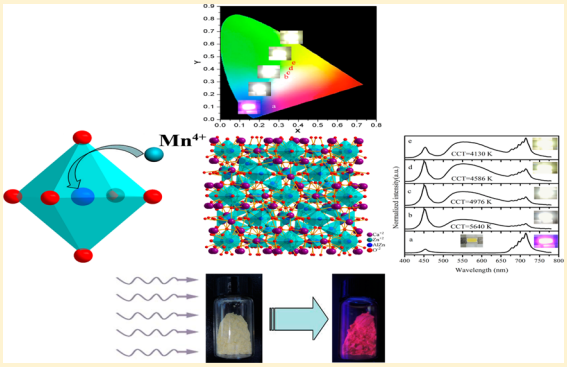

INTRODUCTION

Red-emitting phosphors play a key role in solid-state lighting for illumination applications.[1−10] For example, the major white light-emitting diodes (LEDs) presently in the market are phosphor-converted LEDs (pc-LEDs) made of a blue InGaN chip and a yellow phosphor, $(Y,Gd)_3(Al,Ga)_5O_{12}:Ce^{3+}$ (abbreviated YAG:Ce^{3+}).[11,12] Its luminescence suffers from problems such as cold white light and a low color-rendering index (CRI), which results from the lack of red spectral contribution.[13−15] In addition, the application in artificial lighting for plant cultivation that employs red light covers the spectral region of 650−750 nm. Plants grow better under red LEDs compared to those grown under daylight fluorescent (white) lamps because red light is close to the maximum absorbance for chlorophyll.[16,17] In this regard, searching for a new red phosphor is one of the big challenges in the field of luminescent materials particularly when a red-emitting phosphor is preferred in some occasions with high color purity.

The basic requirements of potential red phosphor for a blue chip scheme are (1) it should have significant absorption in blue;[18,19] (2) it must have high quantum efficiency of the red emission;[20] (3) it must be capable of retaining its luminescent characteristics over long periods at 150 °C.[21] Recently, nonrare earth-based eco-friendly phosphors, Mn^{4+}-doped crystalline host materials, which can be synthesized under milder conditions, have received great interest.[22−30] It usually exhibits broad and strong absorption between 300 and 480 nm and emits light between 600 to 760 nm. Moreover, it avoids using the high price of rare earths and minimizes the cost of the LED device, one of the main obstacles for widespread adoption.

In this contribution, we report on a kind of novel red luminescence material $Ca_{14}Al_{10}Zn_6O_{35}:Mn^{4+}$. The crystal phase formation was refined and determined from X-ray diffraction (XRD) profiles by the Rietveld refinement method. The luminescence properties were investigated by photoluminescence (PL) excitation and emission spectra, decay curves, color coordinates, and thermal quenching properties. We also aim to enhance the luminescence intensity of the $Ca_{14}Al_{10}Zn_6O_{35}:Mn^{4+}$ red phosphor by adding rare earth ions. The results indicate that this may be helpful in developing new red luminescence materials.

EXPERIMENTAL SECTION

Synthesis. The $Ca_{14}Al_{10-x}Zn_6O_{35}$(CAZO):$xMn^{4+}$ phosphors were synthesized by a high-temperature solid-state reaction. The constituent oxides or carbonates $CaCO_3$ (99.9%), ZnO (99.9%), Al_2O_3 (99.9%), and $MnCO_3$ (99.99%) were employed as the raw materials, which were mixed homogeneously by an agate mortar for 30 min, placed in a crucible with a lid, and then sintered in a tubular furnace at 1220 °C for 4 h in air.

Characterization. The phase purity of all samples were identified by powder XRD analysis (Bruker AXS D8), with graphite monochromatized Cu Kα radiation (λ = 0.154 05 nm) operating at 40 kV and 40 mA. Rietveld refinement was performed with Fullprof program package. The scale factor, zero shift, background, and cell parameters were refined. The measurements of PL and photoluminescence excitation (PLE) spectra and diffuse reflectance (DR) spectra were carried out on a Hitachi F4500 spectrometer equipped with a 150 W xenon lamp under a working voltage of 700 V. Thermal quenching studies of the phosphors were measured with a Horiba

Received: July 10, 2014
Published: October 28, 2014

   dx.doi.org/10.1021/ic501641q | *Inorg. Chem.* 2014, 53, 11985−11990

Jobin−Yvon Fluorolog-3 FL3-211 spectrometer equipped with a 450 W xenon lamp as the excitation source. Absolute photoluminescence quantum yields (QYs) were measured by the absolute PL quantum yield measurement system (C9920−02, Hamamatsu Photonics K. K., Japan). The luminescence decay curves were obtained from a Lecroy Wave Runner 6100 digital oscilloscope (1 GHz) using a tunable laser (pulse width = 4 ns, gate = 50 ns) as the excitation source (Continuum Sunlite OPO). The Commission Internationale de l'Eclairage (CIE) chromaticity color coordinates, color rendering index (Ra), and color temperature (CCT) were measured by Starspec SSP6612.

RESULTS AND DISCUSSION

Figure 1 shows the observed (×), calculated (solid line), and difference (bottom) XRD profiles for the Rietveld refinement

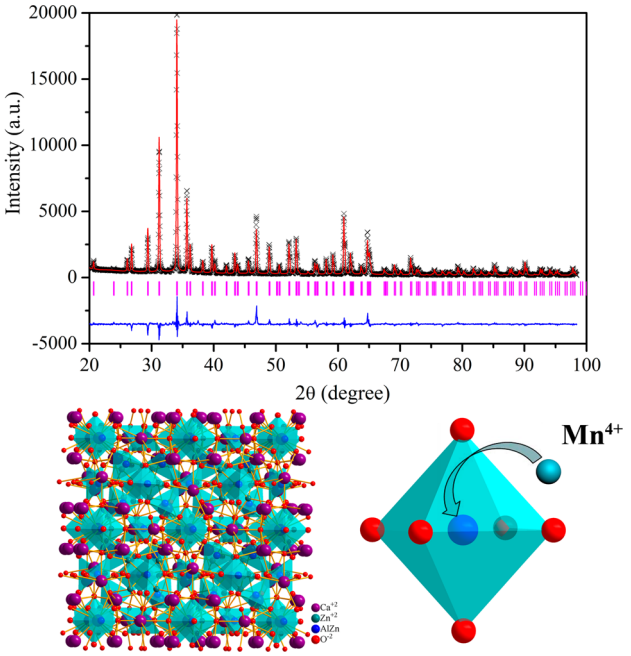

Figure 1. Experimental (×), calculated (solid line), and their difference results (bottom) XRD profiles for the Rietveld refinement of CAZO:Mn^{4+} and a schematic of the CAZO crystal structure.

of CAZO:0.15Mn^{4+} phosphors. The Rietveld refinement results indicate that the doped 0.15 mol Mn^{4+} ions caused any impurity or secondary phases in CAZO host structure. The CAZO:$x$$Mn^{4+}$ crystallizes as a cubic structure with space group $F23$. For CAZO:0.15Mn^{4+} crystal, the lattice parameters were determined to be $a = b = c = 14.8841$ Å and $V = 3297.37$ Å^3, and the refinement finally converged to $R_p = 7.52\%$, $R_{wp} = 9.67\%$, and $\chi^2 = 5.31$. Figure 1 also shows a schematic of the CAZO crystal structure. In the crystal lattice of CAZO, four of the five independent positions occupied by Al and Zn are in tetrahedral coordination, and the fifth independent position is in octahedral coordination. In addition, Ca cation has three different coordination environments. Two of them are six-coordinated in octahedra. The third independent Ca cation is in a seven-coordinated polyhedron. It can be seen that AlO_4 and ZnO_4 tetrahedra (partial disorder) share vertices to form a three-dimensional framework and additional Al and Ca in octahedral voids. It was commonly accepted that Mn^{4+} ions are preferentially accommodated at the Al^{3+} sites in the lattice with an octahedral coordination. Therefore, charge compensations are required due to the different valences of Al^{3+} and Mn^{4+} ions. Murata et al. proposed that a part of Mn ions would have to form Mn^{2+} valence state to compensate charge imbalance,[22] while Pan et al. speculated that Mn^{4+} ions are inclined to form Mn^{4+}−Mn^{4+} ion pairs in the lattice owing to the need in charge compensation.[31] Although the general principles of the charge compensation in Mn-doped phosphors were proposed, the mechanisms of such charge compensation was difficult to prove. In this case, we presume that, like Mn doped in other aluminate,[22,32,33] Mn^{2+} ions may exist and substitute the Al^{3+} sites to keep the electroneutrality of the compound.

As expected for an oxide host, the d−d transition of manganese ion within its $3d^3$ electron configuration is an identified red light at ∼650 nm with broad absorption band in visible region. Figure 2 shows the PLE and PL spectra of

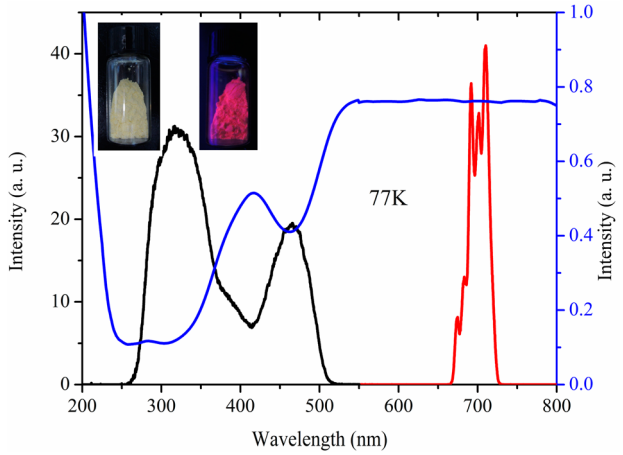

Figure 2. PLE and PL spectra of CAZO:Mn^{4+} phosphors at 77 K and the DR spectrum at room temperature. (inset) Photograph of the obtained CAZO:Mn^{4+} phosphors under illumination of white light (left) and UV (365 nm) light (right).

CAZO:Mn^{4+} phosphors at 77 K and the DR spectrum at room temperature. The PLE spectra exhibit two typical absorption peaks at 318 and 462 nm, while one is in the region of 400−500 nm, which is attributed to the $^4A_2 \rightarrow {}^4T_2$ transitions of Mn^{4+} ion in octahedral coordination. The other is between 300 and 400 nm, which is due to the existence of a charge transfer band (CTB) of Mn^{4+}−O^{2-}. Excitation into this absorption band at 460 nm gives a luminescence band located at ∼692, 701, and 708 nm due to the $^2E \rightarrow {}^4A_2$ transition of Mn^{4+} ions. A red shift of emission occurs in our prepared phosphors compared to $Sr_2MgAl_{22}O_{36}$ Mn^{4+} and $CaAl_{12}O_{19}$:Mn^{4+}.[22,25] The PL peak of the CAZO:Mn^{4+} is lower than that of oxides host, implying a stronger crystal field on Mn^{4+} in this host. Those PLE spectra suggest that CAZO:Mn^{4+} phosphor can be excited by UV (310−380 nm), near UV (380−420 nm), and blue (420−480 nm) LED chips. As shown in Figure 2 inset, very bright red luminescence under the illumination of UV (365 nm) light can be clearly seen, indicating CAZO:Mn^{4+} can be used as a promising phosphor as a red component applied to LED technology.

Figure 3 shows PL spectra of CAZO:$x$$Mn^{4+}$ phosphors (x = 0.05, 0.1, 0.15, 0.2, 0.25, 0.3) at room temperature (λ_{ex} = 460 nm). The PL spectra exhibit a red emission centered at 700 nm, which is imputed to the $^2E \rightarrow {}^4A_2$ of the Mn^{4+} ion. The optimal Mn^{4+} dopant content is found to be $x = 0.15$, and the PL intensity increases with increasing x when $x < 0.15$. For samples with Mn^{4+} dopant content higher than 0.15, concentration quenching is observed, and the PL intensity is found to

dx.doi.org/10.1021/ic501641q | Inorg. Chem. 2014, 53, 11985−11990

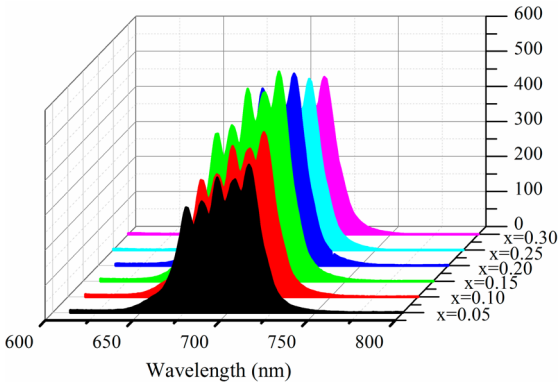

Figure 3. PL spectra of CAZO:xMn^{4+} phosphors (x = 0.05, 0.1, 0.15, 0.2, 0.25, 0.3) at room temperature (λ_{ex} = 460 nm).

decrease with increasing Mn^{4+} dopant content. The cross energy transfer and nonradiative relaxation become predominant when the concentration of Mn^{4+} reaches a certain concentration. As reported, the formation of Mn^{4+}−Mn^{4+} pairs in connection with O^{2-} impurities would significantly reduce the luminescence efficiency of Mn^{4+}.[31] This phenomenon is inconsistent with our results in Figure 3. Therefore, this may be evidence that mechanisms of such charge compensation result from the formation of Mn^{2+} rather than Mn^{4+}−Mn^{4+} ion. The decay curves of Mn^{4+}-doped CAZO:xMn^{4+} (x = 0.05−0.3) phosphors monitored at 700 nm are displayed in Figure 4. The

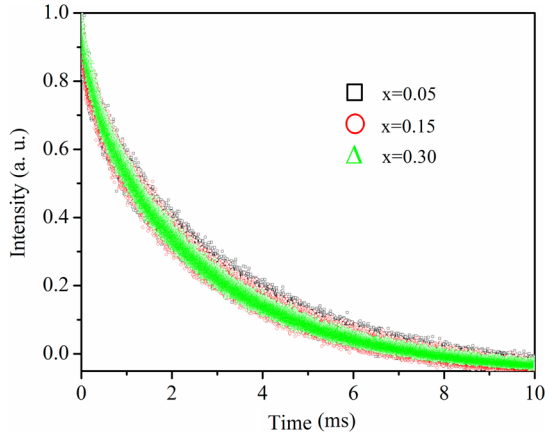

Figure 4. Decay curves of Mn^{4+}-doped CAZO:xMn^{4+} (x = 0.05−0.3) phosphors monitored at 700 nm.

fluorescence lifetime of the optimized red-emitting CAZO:0.15Mn^{4+} phosphor is ∼1.49 ms, which is longer than that of $CaAl_{12}O_{19}$:Mn^{4+} phosphor (∼0.83 ms). The calculated lifetimes do not change significantly with rising amounts of Mn^{4+} ions in the matrix.

To evaluate the potential as color converter in LEDs, the thermal quenching behavior was measured. Figure 5a depicts the temperature-dependent emission spectra. Upon heating the sample to 150 °C, at which temperature the white LEDs usually work, the emission intensity gradually decreased, until it remained at ∼88% of that the initial emission intensity. The decrease in emission intensity with increasing temperature can be explained by thermal quenching at configurational coordinate diagram.[34] The activation energy can be described by the equation

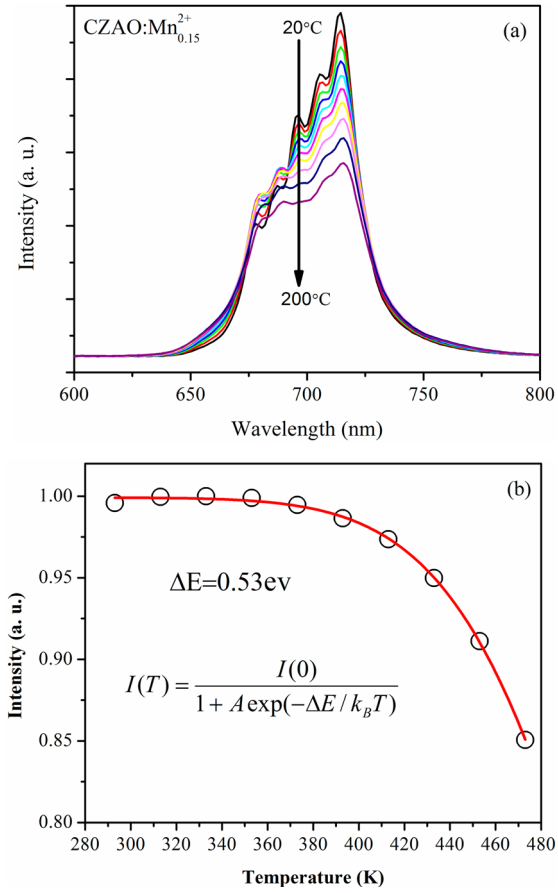

Figure 5. (a) The temperature-dependent emission intensity of the optimized CAZO:0.15Mn^{4+} samples. (b) Integrated red PL intensity as a function of temperature.

$$I(T) = \frac{I(0)}{1 + A\ \exp(-\Delta E/k_B T)} \quad (1)$$

where $I(0)$ and $I(T)$ is the initial intensity and the intensity at temperature T, ΔE is the activation energy, A is a constant, and k_B is Boltzmann constant. The experimental data are well-fitted by eq 1, as shown in Figure 5b. An activation energy of Mn^{4+} in CAZO:0.15Mn^{4+} is 0.53 eV. This value is much higher than that of Mn^{4+} in $CaAl_4O_7$ but lower than that of Mn^{4+} in K_2TiF_6.[19,27]

To demonstrate the application of CAZO:Mn^{4+} phosphors, white LED lamps were fabricated using a 460 nm blue chip combined with a blend of yellow-emitting YAG:Ce^{3+} and red-emitting CAZO:0.15Mn^{4+} phosphors driven by 20 mA current. Figure 6 displays the electroluminescence (EL) spectrum of red/white emitting LEDs composed of a 460 nm blue chip and a phosphor blend of YAG:Ce^{3+} and CAZO:0.15Mn^{4+} in various mixing ratios. With increasing the weight ratio of CAZO:Mn^{4+}, the EL spectrum of CAZO:Mn^{4+} at 700 nm increases, and the CCT continuously decreases from 5640 to 4130 K. Red and warm-white lights are successfully created with samples a and e, respectively. Figure 7 shows the CIE chromaticity diagram of red/white LEDs of our devices. By weight ratio tuning, the chromaticity coordinates (x, y) of LEDs vary from (point a, (0.26, 0.10)) through white (point c, (0.33, 0.35)) and then to warm white-light (point e, (0.39, 0.44)) region. The inset shows the photograph of the LED package driven by 20 mA current. The white LEDs fabricated in this study (point d)

dx.doi.org/10.1021/ic501641q | Inorg. Chem. 2014, 53, 11985−11990

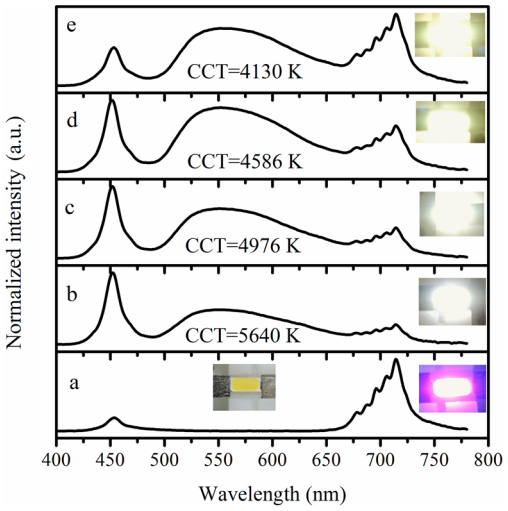

Figure 6. (a) The EL spectrum of red-emitting LEDs composed of a 460 nm blue chip and CAZO:0.15Mn^{4+}. The EL spectrum of white-emitting LEDs composed of a 460 nm blue chip and a phosphor blend of YAG:Ce^{3+} and CAZO:0.15Mn^{4+} in various mixing ratios with CCT of (b) 5640, (c) 4976, (d) 4586, (e) 4130 K, respectively. (insets) The photograph of the LED lamp package driven by 20 mA current.

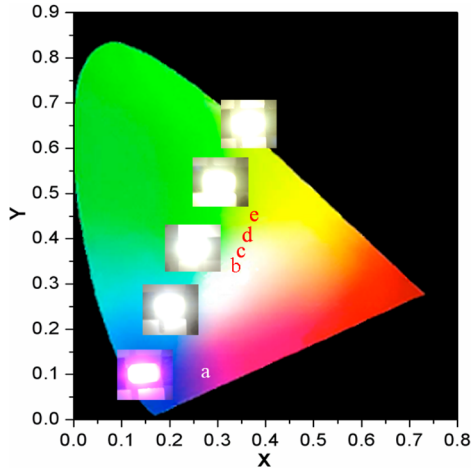

Figure 7. CIE chromaticity diagram of red/white LEDs of a, b, c, d, e driven by 20 mA current.

show lower CCT values (4586 K for CAZO:Mn^{4+}, 7272 K for YAG:Ce^{3+}), demonstrating that CAZO:Mn^{4+} has potential applications in the white LEDs with warm white light.

As the local environment has influence on the optical properties of the activator ions, we first used Zn^{2+} as a network modifier ion. Replacing Zn with Mg, as shown in Figure 8, resulted in the slight decrease of luminescence intensity under excitation at 460 nm. This phenomenon was presumably caused by the incompleteness of the solid-state reaction. As shown in Figure 9, a certain amount of impurity $Ca_3MgAl_4O_{10}$ (maybe incorporating a small amount of calcium aluminate) existed. Decrease in the amount of the luminescent material $Ca_{14}Al_{9.85}Zn_6O_{35}$:0.15$Mn^{4+}$ is likely the reason for the decrease of the luminescence intensity. By the way, the XRD peak slightly shifted to low-angle regions with adding Mg^{2+}, reflecting the substitution of Zn^{2+} by Mg^{2+}. For the ionic radius (r) of Mg^{2+} (r = 0.71 Å or CN = 4) is bigger than that of Zn^{2+} (r = 0.60 Å or CN = 4) so as to enlarge the lattice. Furthermore, we attempt to improve the luminescence

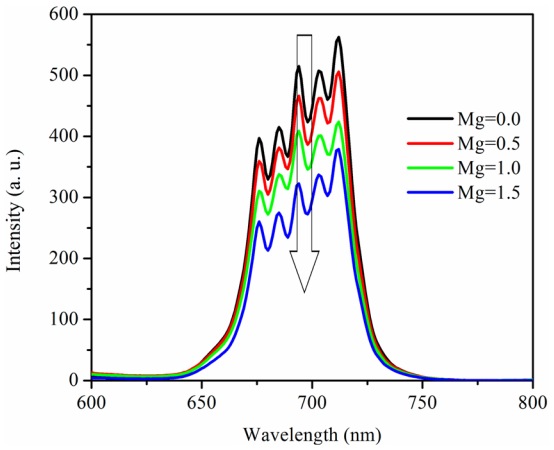

Figure 8. PL spectra of $Ca_{14}Al_{10}Zn_{6-y}Mg_yO_{35}$:0.15$Mn^{4+}$ under excitation at 460 nm with y = 0, 0.5, 1, 1.5.

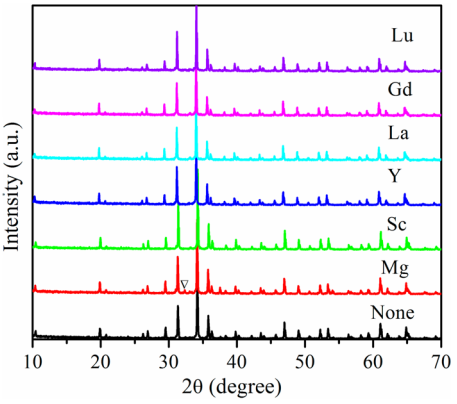

Figure 9. XRD pattern of the $Ca_{14}Al_{9.85}Zn_{5.5}Mg_{0.5}O_{35}$:0.15$Mn^{4+}$ and $Ca_{13.5}Ln_{0.5}Al_{9.85}Zn_6O_{35}$:0.15$Mn^{4+}$ (Ln = Sc, Y, La, Gd, and Lu) samples.

properties by codoping Ln^{3+} (Ln = Sc, Y, La, Gd, and Lu) instead of Ca^{2+}. Figure 9 also shows the XRD patterns of the $Ca_{13.5}Ln_{0.5}Al_{9.85}Zn_6O_{35}$:0.15$Mn^{4+}$ samples. All the recorded diffraction peaks could be indexed according to the $Ca_{14}Al_{10}Zn_6O_{35}$, indicating that the samples were of single phase and isostructural to that given in JCPDS card no. 50−0426.

Figure 10a exhibits the PL spectra of CAZO:0.15Mn^{4+} without any dopant and doped various Ln^{3+} (Ln = Sc, Y, La, Gd, and Lu) ions. It can be seen that the emission spectra profiles of the Ln^{3+}-substituted phosphors under 460 nm excitation are identical with that of CAZO:$x$$Mn^{4+}$, but emission intensities are changed with Ln^{3+} substitution. Figure 10b gives the values of the relative intensity and the absolute quantum yields of $Ca_{13.5}Ln_{0.5}Al_{9.85}Zn_6O_{35}$ doped with different lanthanide ions. We have observed that the tendency of the absolute quantum yield is consistent with that of the relative intensity. Introduction of Y, La, and Gd ions into the $Ca_{13.5}Ln_{0.5}Al_{9.85}Zn_6O_{35}$:0.15$Mn^{4+}$ structure decreased the most effective intensity from all used Ln^{3+} dopants. The absolute QYs of CAZO:0.15Mn^{4+} and $Ca_{13.5}Ln_{0.5}Al_{9.85}Zn_6O_{35}$:0.15$Mn^{4+}$ (Ln = Sc, Y, La, Gd, and Lu) are determined to be 50.7, 52.0, 27.5, 33.6, 38.7, and 59.8%, respectively. Only the addition of Sc^{3+} and Lu^{3+} increases the emission intensity and the absolute QY. In the view of effective ionic radii, [Ca^{2+} (0. 100 Å, CN = 6), Sc^{3+} (0.075 Å, CN = 6), Y^{3+} (0.104 Å, CN = 6), La^{3+} (0.103

dx.doi.org/10.1021/ic501641q | Inorg. Chem. 2014, 53, 11985−11990

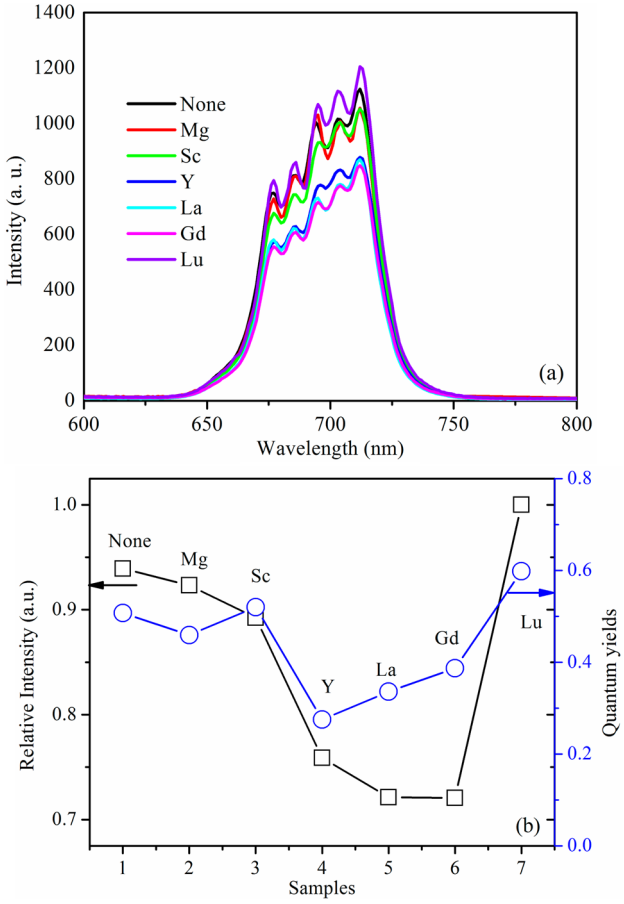

Figure 10. (a) The PL spectra of CAZO:0.15Mn^{4+} without any dopant and doped by various ions. (b)The corresponding relative intensity and the absolute quantum yields.

Å, CN = 6), Gd^{3+} (0.094 Å, CN = 6), and Lu^{3+} (0.086 Å, CN = 6)], it seems that replacement Ca^{2+} sites with ions with smaller radius can enhance the luminous efficiency; however, the origin of this phenomenon is not clearly understood at present. Figure 11 shows the typical luminescence decay curves of the $Ca_{13.5}Ln_{0.5}Al_{9.85}Zn_6O_{35}$:0.15$Mn^{4+}$ and $Ca_{14}Al_{9.85}Zn_{5.5}Mg_{0.5}O_{35}$:0.15$Mn^{4+}$ samples under the excitation of 355 nm. It is found that the lifetimes of the samples decrease with Ln^{3+} substitution, especially of the Y, La, and Gd ions. As we know, the lifetime τ is dominated by the radiative transition rate W_R, and the nonradiative decay rate W_{NR}, which can be written as $\tau = 1/(W_R + W_{NR})$. Therefore, we speculated that the nonradiative rate increases greatly with Y^{3+}, La^{3+}, and Gd^{3+} substitution at the Ca^{2+} site, leading to the quantum efficiency reduction.

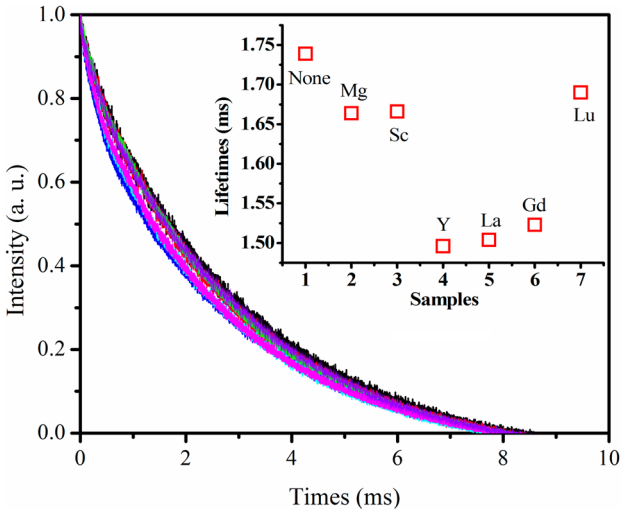

Figure 11. Typical luminescence decay curves of the $Ca_{14}Al_{9.85}Zn_{5.5}Mg_{0.5}O_{35}$:0.15$Mn^{4+}$, $Ca_{13.5}Ln_{0.5}Al_{9.85}Zn_6O_{35}$:0.15$Mn^{4+}$, and CAZO:0.15$Mn^{4+}$ samples under the excitation of 355 nm.

Anyway, replacement of the constituent elements of $Ca_{13.5}Ln_{0.5}Al_{9.85}Zn_6O_{35}$:0.15$Mn^{4+}$ phosphor with other ions, especially replacing with Lu, should be further studied by optimizing the synthetic conditions.

CONCLUSIONS

In summary, a new, highly efficient deep red-emitting phosphor $Ca_{14}Al_{10}Zn_6O_{35}$:Mn^{4+} was successfully synthesized via conventional high-temperature solid-state reaction. The prepared phosphor can be efficiently excited by near-UV and blue light from 300 to 500 nm and exhibits a deep red emission at a region of 650−750 nm. The optimum concentration of Mn^{4+} ions in CAZO:xMn^{4+} was determined to be x = 0.15. Thermal stability study of the red emission Mn^{4+} ions is investigated and ensures the efficiency and color of pcWLEDs. Moreover, by combining the synthesized $Ca_{14}Al_{10}Zn_6O_{35}$:Mn^{4+} phosphors with YAG:Ce and the blue InGaN LED chip, warm white light has been created. In addition, introduction of the lanthanide ions (especially dopants Sc^{3+} and Lu^{3+} ions) into the $Ca_{14}Al_{10}Zn_6O_{35}$ structure enhances the absolute quantum yields.

AUTHOR INFORMATION

Corresponding Authors

*E-mail: hpyou@ciac.ac.cn. Fax: +86-431-85698041. Phone: +86-431-85262798. (H.-P.Y.)

*E-mail: wlv@ciac.ac.cn. (W.L.)

Notes

The authors declare no competing financial interest.

ACKNOWLEDGMENTS

This work is financially supported by the National Natural Science Foundation of China (Grant Nos. 21271167 and 11304309), the Fund for Creative Research Groups (Grant No. 21221061), and the National Basic Research Program of China (973 Program, Grant No. 2014CB6438003).

REFERENCES

(1) Xie, R. J.; Hirosaki, N.; Suehiro, T.; Xu, F. F.; Mitomo, M. *Chem. Mater.* **2006**, *18*, 5578−5583.

(2) Piao, X.; Machida, K.; Horikawa, T.; Hanzawa, H.; Shimomura, Y.; Kijima, N. *Chem. Mater.* **2007**, *19*, 4592−4599.

(3) Wang, Z. L.; Liang, H. B.; Gong, M. L.; Su, Q. *Solid State Lett.* **2005**, *8*, H33−H35.

(4) Huang, C. H.; Kuo, T. W.; Chen, T. M. *ACS Appl. Mater. Interfaces.* **2010**, *2*, 1395−1399.

(5) Sohn, K. S.; Park, D. H.; Cho, S. H.; Kwak, J. S.; Kim, J. S. *Chem. Mater.* **2006**, *18*, 1768−1772.

(6) Yang, X. Y.; Liu, J.; Yang, H.; Yu, X. B.; Guo, Y. Z.; Zhou, Y. Q.; Liu, J. Y. *J. Mater. Chem.* **2009**, *19*, 3771−3774.

(7) Liu, Y. F.; Zhang, X.; Hao, Z. D.; Liu, X. Y.; Wang, X. J.; Zhang, J. H. *J. Mater. Chem.* **2011**, *21*, 6354−6358.

(8) Li, G. G.; Geng, D. L.; Shang, M. M.; Zhang, Y.; Peng, C.; Cheng, Z. Y.; Lin, J. *J. Phys. Chem. C* **2011**, *115*, 21882−21892.

(9) Liu, Y. F.; Zhang, X.; Hao, Z. D.; Wang, X. J.; Zhang, J. H. *Chem. Commun.* **2011**, *47*, 10677−10679.
(10) Oh, J. H.; Yang, S. J.; Do, Y. R. *Light: Sci. Appl.* **2014**, *3*, e141−e149.
(11) Nakamura, S.; Fasol, G. *The Blue Laser Diode;* Springer: Berlin, Germany, 1996.
(12) Nakamura, S. *MRS Bull.* **2009**, *34*, 101−107.
(13) Kim, J. S.; Jeon, P. E.; Park, Y. H.; Choi, J. C.; Park, H. L.; Kim, G. C.; Kim, T. W. *Appl. Phys. Lett.* **2004**, *85*, 3696−3698.
(14) Hao, Z. D.; Zhang, J. H.; Zhang, X.; Sun, X. Y.; Luo, Y. S.; Lu, S. Z.; Wang, X. J. *Appl. Phys. Lett.* **2007**, *90*, 261113−1−3.
(15) Xie, R. J.; Hirosaki, N.; Takeda, T. *Appl. Phys. Express.* **2009**, *2*, 022401−022403.
(16) Goins, G. D.; Yorio1, N. C.; Sanwo M. M. Brown, C. S. *J. Exp. Bot.* **1997**, *48*, 1407−1413.
(17) Tamulaitis, G.; Duchovskis, P.; Bliznikas, Z.; Breive, K.; Ulinskaite, R.; Brazaityte, A.; Novickovas, A.; Zukauskas. *J. Phys. D: Appl. Phys.* **2005**, *38*, 3182−3187.
(18) Li, X. F.; Budai, J. D.; Liu, F.; Howe, J. Y.; Zhang, J. H.; Wang, X. J.; Gu, Z. J.; Sun, C. J.; Meltzer, R. S.; Pan, Z. W. *Light: Sci. Appl.* **2013**, *2*, e50−e58.
(19) Daicho, H.; Iwasaki, T.; Enomoto, K.; Sasaki, Y.; Maeno, Y.; Shinomiya, Y.; Aoyagi, S.; Nishibori, E.; Sakata, M.; Sawa, H.; Matsuishi, S.; Hosono, H. *Nat. Commun.* **2012**, *3*, 1132.
(20) Zeuner, M.; Hintze, F.; Schnick, W. *Chem. Mater.* **2009**, *21*, 336−342.
(21) Suehiro, T.; Hirosaki, N.; Xie, R. J. *ACS Appl. Mater. Interfaces.* **2011**, *3*, 811−816.
(22) Murata, T.; Tanoue, T.; Iwasaki, M.; Morinaga, K.; Hase, T. *J. Lumin.* **2005**, *114*, 207−212.
(23) Okamoto, S.; Yamamoto, H. *J. Electrochem. Soc.* **2010**, *157*, J59−J63.
(24) Brik, M. G.; Pan, Y. X.; Liu, G. K. *J. Alloys Compd.* **2011**, *509*, 1452−1456.
(25) Cao, R. P.; Peng, M. Y.; Song, E. H.; Qiu, J. R. *ECS J. Solid State Sci. Technol.* **2012**, *1*, R123−R126.
(26) Peng, M. Y.; Yin, X. W.; Tanner, P. A.; Liang, C. Q.; Li, P. F.; Zhang, Q. Y.; Qiu, J. R. *J. Am. Ceram. Soc.* **2013**, *96*, 2870−2876.
(27) Li, P. F.; Peng, M. Y.; Yin, X. W.; Ma, Z. J.; Dong, G. P.; Zhang, Q. Y.; Qiu, J. R. *Opt. Express.* **2013**, *21*, 18943−18948.
(28) Jiang, X. Y.; Pan, Y. X.; Huang, S. M.; Chen, X.; Wang, J. G.; Liu, G. K. *J. Mater. Chem. C* **2014**, *2*, 2301−2306.
(29) Du, M. H. *J. Mater. Chem. C* **2014**, *2*, 2475−2481.
(30) Zhu, H. M.; Lin, C. C.; Luo, W.; Shu, S.; Liu, Z.; Liu, Y.; Kong, J.; Ma, E.; Cao, Y.; Liu, R. S.; Chen, X. *Nat. Commun.* **2014**, *5*, 4312.
(31) Pan, Y. X.; Liu, G. K. *Opt. Lett.* **2008**, *33*, 1816−1818.
(32) Lu, J.; Pan, Y.; Wang, J.; Chen, X.; Huang, S.; Liu, G. *RSC Adv.* **2013**, *3*, 4510−4513.
(33) Li, Y.; Li, Y. Y.; Sharafudeen, K.; Dong, G. P.; Zhou, S. F.; Ma, Z. J.; Peng, M. Y.; Qiu, J. R. *J. Mater. Chem. C* **2014**, *2*, 2019−2027.
(34) Henderson, B.; Imbush, G. G. *Optical Spectroscopy of Inorganic Solids;* Clarendon: Oxford, U.K., 1989.